JOURNAL OF APPLIED ELECTROCHEMISTRY 14 (1984) 653–661

Primary current distribution in a two-dimensional model cell composed of an electrode with an open part

YOSHINORI NISHIKI

Research and Development Center, Permelec Electrode Ltd, 1159, Ishikawa, Fujisawa, Kanagawa prefecture, 252 Japan

KOICHI AOKI, KOICHI TOKUDA, HIROAKI MATSUDA

Department of Electronic Chemistry, Graduate School at Nagatsuta, Tokyo Institute of Technology, Nagatsuta, Midori-ku, Yokohama, 227 Japan

Received 18 October 1983; revised 19 December 1983

A two-dimensional model for industrial production-type cells in which electrodes have holes for releasing gas bubbles to the back side of the electrodes and a separator located between the working- and counter-electrodes is proposed in conjunction with some geometrical parameters of the electrode and the cell. The primary current distribution in this model was calculated for a series of values of the parameters by the finite element method. The current distribution in the cell with the separator is quite different from that without the separator. Variations of the ohmic potential drop with the parameters reveal that the cell resistance is determined not only by the interelectrode distance but also by the per cent open area and in some cases by the superficial surface area. The partitions of the total current into the currents on the front, the back and the intermediate sides of the working-electrode are obtained as functions of the per cent open area and the superficial surface area. These results may be useful for estimating the performance of the electrode.

Nomenclature

b distance from the back wall to the back side of the working-electrode
d_1 distance between the front side of the working-electrode and the separator (or the counter electrode when cell has no separator)
d_2 width of the separator
I total current per half pitch
L length of a real electrolysis cell
n coordinate perpendicular to the boundary of the model cell
o_p per cent open area, given by Equation 1 for the present model
p pitch, i.e. twice the length of the unit cell
R equivalent unit-cell resistance defined by Equation 13
R_t total cell resistance
r ratio of the average current density on each side of the working-electrode to that of the counter-electrode
s superficial surface area, given by Equation 2 for the present model
t thickness of the working electrode
u_k function defined by Equation 10
v test function
w width of the working electrode
x abscissa located on the cell model
y ordinate located on the cell model
$d\gamma$ infinitesimal length on the boundary
ρ_1 resistivity of the solution phase
ρ_2 resistivity of the separator
ϕ potential
ϕ^* potential at the working electrode
Γ linear integration contour along I0, AH or EFDH
Ω double integration space in the solution or the separator phase

0021–891X/84 $03.00 + .12

Subscripts

k solution ($k = 1$) or separator ($k = 2$)
i interface between solution and separator
e working-electrode or counter-electrode

1. Introduction

One of the significant factors which causes an increase in ohmic potential drop in industrial electrolytic cells is cell configuration or electrode geometry. Electrodes employed at present in well-developed factories have been designed to minimize the ohmic drop and there are several types of geometry, e.g. an expanded electrode, a louvre-type electrode, a perforated electrode and a woven electrode. Most of them have voids or holes through which a solution and evolving gas bubbles pass to be removed from the interelectrode space. Voids in the working-electrode, playing a role in promoting mass transport, bring about non-uniform current distribution because the inside wall of the voids and the back surface of the working-electrode as well as the electrode surface facing a counter-electrode act as active electrode. Therefore ohmic potential drop may be different from that estimated by the uniform current distribution. It is of interest and of significance to examine to what extent the inside of a void and the back side of the electrode take part in electrolysis and how much the ohmic loss is due to the voids in an electrode. These problems require knowledge of the potential distribution in a cell.

Potential distribution can be obtained by a solution of the Laplace equation. Kasper, for the first time in the electrochemical field, calculated current distributions in the point–plane system, in the line–plane system and in two-dimensional rectangular enclosures [1–3]. Ishizaka and Matsuda [4–7] and Wagner [8, 9] extended his approach to rectangular cells with more complicated geometries by the use of the Schwarz–Christoffel transformation and further examined the effects of the overvoltage on the current distribution. Hine [10] evaluated the effects of the back wall in a rectangular cell on the current distribution. Recently, Vaaler [11] approximated the resistances of a cell and an electrode as a three-dimensional grid network and calculated current distribution in the cell. The effects of gas evolution on current distribution and cell resistance have been presented by various authors (Tobias [12], de la Rue and Tobias [13], Sides and Tobias [14, 15], Hine *et al.* [16, 17], Hine and Murakami [18, 19], Nagy [20], Kuhn *et al.* [21], Kreysa and Külps [22], Jorne and Louvar [23], Janssen *et al.* [24], Vogt [25], Lanzi and Savinell [26]). Since these papers are concerned with an increase in the ohmic potential drop due to evolving gas bubbles, detailed dependence of current distribution on a cell geometry has not been described systematically. Therefore, it is necessary to examine such dependence in a cell composed of electrodes having voids in order to obtain an optimum electrolysis condition from the viewpoint of cell geometry.

This paper is devoted to theoretical examination of the geometrical effect by computing the primary current distribution in a solution and a separator phase with a uniform resistivity when the geometries of the electrode and the cell are varied in the two-dimensional model cell. The computational method employed is the finite element method, which was first developed in the field of structural stress analysis and has since been applied extensively to various other fields. The finite element method has recently been used in some electrochemical problems concerned with cell and electrode geometry [27–29].

2. A choice of model

There are several significant parameters that determine the configuration of the cell and geometry of the electrode. One is the per cent open area, o_p, which is defined as the percentage ratio of the total projected area of holes to the projected area of the electrode. Another parameter is the superficial surface area, s, which is expressed as the ratio of the electrode area in contact with the electrolyte to the projected area of the electrode. The other parameters are thickness of the electrode, width of the electrode and pitch, i.e. the length of the unit cell. It must be noted that these parameters are not necessarily independent of each other. In connection with the location of the electrode in the cell or an arrangement of the cell, there are two more parameters. One of these is the distance between the working-electrode and the separator (e.g. an ion exchange membrane or a diaphragm). The other is the width of the cell, i.e.

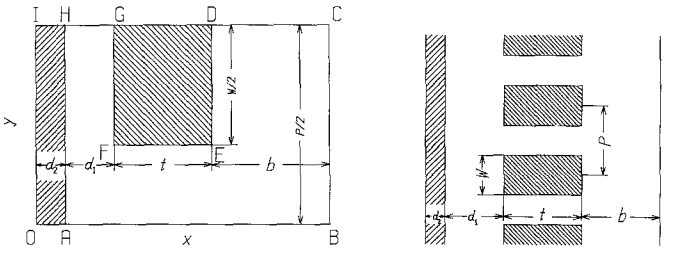

Fig. 1. Two-dimensional cell model (a) unit cell, (b) head-to-head and tail-to-tail connections of the unit cells, which corresponds to an assembly of strip-shaped electrodes.

the distance between the separator and the back wall. Ultimately, an adequate combination of these parameters might yield a cell with high performance.

Taking into account the implication of the parameters described above, we set up a two-dimensional model of the cell configuration, as shown in Fig. 1a. The region encircled with ABCDEFGH is a phase filled with electrolyte solution. The domain, DEFG, represents the working-electrode whereas the region surrounded by OAHI is the counter-electrode or the separator to the left of which the counter-electrode is attached. The other sides, AB, BC, CD and GH, are insulated walls. Head to head and tail to tail connections of the model cell yield the cross section of the assembly of the strip-shaped electrodes, as shown in Fig. 1b. The dimensions of the cell are shown in Figs. 1a, b, where the pitch, p, is used as a characteristic length of the model. The important characteristics of the electrode geometry are revealed in the per cent open area, the superficial surface area and the pitch. In terms of these dimensions, the per cent open area, o_p, and the superficial surface area, s, can be expressed, respectively, as

$$o_p = 100(p - w)/p \tag{1}$$

$$s = 2(w + t)/p \tag{2}$$

The per cent open area is equivalent to the complement of w in this model.

There is a solution between the counter-electrode and the separator in a real cell. It is possible to replace the sum of the resistances of the separator and the solution by an equivalent resistance of the separator. Therefore this model approximates a real cell so far as evaluation of the current distribution in the vicinity of the working-electrode is concerned.

This model has been proposed in the light of the configuration of the assembly of strip-shaped electrodes. However, it is possible to readily reduce the geometry of the real cell, which has some known values for the per cent open area, the superficial surface area and the thickness of the electrode (e.g. a perforated electrode), to the proposed model by the use of Equations 1 and 2.

3. Computation of current distribution

It is possible to regard the cell without a separator as a special case of the cell with a separator, the resistance of which has the same value as that of the solution. Hence, only the cell with a separator is dealt with in this section.

We shall obtain the primary current distribution in the model cell on the assumptions that the solution and the separator have uniform resistivities over each phase and that the resistances of the working- and the counter-electrodes are small enough to be negligible in comparison with those of the solution and the separator. Therefore, potential is distributed only in the solution and in the separator. The potential, ϕ, in both phases is expressed by the two-dimensional Laplace equation given by

$$\partial^2\phi/\partial x^2 + \partial^2\phi/\partial y^2 = 0 \tag{3}$$

where x and y denote the coordinates depicted in Fig. 1a. The potential at the working-electrode is taken to have a constant value, ϕ^*, while the potential at the counter-electrode is assumed to be zero, i.e.

$$\phi = \phi^* \qquad \text{on the sides DEFG} \tag{4}$$

$$\phi = 0 \qquad \text{on the side OI} \tag{5}$$

Since there is no sink or source of current at the interface between the separator and the solution, the current density in the solution is equal to that in the separator at the interface, i.e.

$$\rho_2(\partial\phi_1/\partial x) = \rho_1(\partial\phi_2/\partial x) \qquad \text{on the side AH} \tag{6}$$

where subscripts 1 and 2 denote the solution and the separator, respectively. There is, in general, a membrane potential at the interface when the separator is an ion exchange membrane. It is assumed here that the membrane potential does not vary with current density. Then the potential distribution is the same as one without a membrane except for the constant value of the membrane potential. Hence the membrane potential is taken to be zero in this paper. Potentials in both the phases at the interface are expressed by

$$\phi_2 = \phi_1 \qquad \text{on the side AH} \tag{7}$$

On the sides of the insulated walls, the potential gradient is zero:

$$\partial\phi/\partial n = 0 \qquad \text{on sides OB, BC, CD and GI} \tag{8}$$

where n denotes the coordinate perpendicular to the wall.

Since our target is to obtain the relation of the potential distributions with various configurations of the cell, it is necessary to employ a computational method which can bear rather arbitrary variations of cell geometry. One of the most flexible methods is the finite element method [30].

We solve the boundary value problem expressed by Equations 3–8 using the conventional finite element method [30]. Multiplying Equation 3 by a test function $v = v(x, y)$, integrating it over the solution or the separator phase by application of Green's theorem and inserting the boundary condition (Equation 7) into the resulting equation yields:

$$\int_{\Gamma_i} (\pm 1)\,(\partial\phi/\partial x)v\,\mathrm{d}\gamma + \int_{\Gamma_e} (\partial\phi/\partial n)v\,\mathrm{d}\gamma - u_k = 0 \tag{9}$$

with

$$u_k = \int\int_{\Omega_k} [(\partial\phi_k/\partial x)(\partial v/\partial x) + (\partial\phi_k/\partial y)(\partial v/\partial y)] \times \mathrm{d}x\,\mathrm{d}y \tag{10}$$

The upper and lower signs in the first term of Equation 9 are for the separator and the solution phase, respectively. Multiplying Equation 9 by ρ_1 for the upper sign and by ρ_2 for the lower sign and adding these two equations using Equation 6, we obtain

$$\rho_2 \int_{\mathrm{DEFG}} (\partial\phi/\partial n)v\,\mathrm{d}\gamma + \rho_1 \int_{\mathrm{IO}} (\partial\phi/\partial n)v\,\mathrm{d}\gamma = \rho_2 u_1 + \rho_1 u_2 \tag{11}$$

The solution and the separator phases were subdivided into square elements of the same size. The reason for adopting the square element is that it is possible to easily alter the configuration of the cell only by renumbering the element numbers without any assignment of a coordinate to each node. We are not interested in local variations of potential distribution or current density but are concerned with the global features of distribution and the total flux. Therefore the linear interpolating function, which is the simplest and also enhances computation speed, was used to approximate the equation in each element. A global matrix was assembled directly by the stiffness method and was arranged in the form of a banded and symmetric matrix. When the Dirichlet conditions given by Equations 4 and 5 are inserted into this matrix, line components in the matrix corresponding to the Dirichlet conditions should be taken to be zero. Otherwise simultaneous equations might be singular. The set of simultaneous equations involving the Dirichlet conditions was solved by the Gauss elimination method. When values thus obtained at all nodes are substituted into the matrix corresponding to the right hand side of Equation 11, the resulting equation divided by $\rho_1\rho_2$ is reduced to the simultaneous equations with respect to the current density expressed by $(\partial\phi/\partial n)/\rho_k$. These simultaneous equations were solved again by the Gauss elimination method. It is also possible to obtain the current density by the difference between values at adjacent nodes. We found, however, that values of the current density obtained by the difference method are less accurate than those by the present method, therefore we did not use the difference method. The total current, I, i.e. the sum of the current densities at all nodes of the boundaries is expressed by

$$I = \int_{\mathrm{DEFG}} (\partial\phi_1/\partial n)\,\mathrm{d}\gamma/\rho_1 \tag{12}$$

The integral of this equation was calculated by Simpson's 1/3 rule.

All computer programs were coded in standard Fortran IV. Since the global matrix is banded and symmetric, only the upper half elements of the

banded part were loaded in computer memories. In order to check whether our computer program was reasonable or not, we computed with this program the current distribution in the model cell wherein lengths of EF and FG were taken to be $4 \times d_1$. This current distribution was compared with the distribution around the corner in the T-shaped ditch for which an exact expression has been obtained analytically using the Schwarz–Christoffel transformation [31]. The maximum deviation from the analytical solution, which occurred at the node next to the corner, was within 1% when the ratio of the length of the square element to d_1 was 0.1. This fact indicates that the current density even in the vicinity of the corner can be obtained reasonably, though it is impossible to obtain the exact current density at the corner because of its singularity.

The total current, I, defined by Equation 12 should equal the total currents flowing through the surface of the counter-electrode and also through the interface between the solution and the separator. We used this equivalency as a criterion of verification of the computation and found that three total currents were in agreement within errors of 1.5%.

The errors involved in the calculated potential are diminished in general with an increase in the number of elements. However, the accuracy sometimes falls with an increase in the number of elements because of the accumulation of round-off errors during iteration of the computation. From our tentative and empirical computation, the minimum error seems to be achieved when the number of elements is from 1500 to 2500, which corresponds to less than 1 megabyte capacity in IC-memory including the load module for the Fortran source program.

4. Results and discussion

4.1. *Current distribution*

The potential distributions in cells with and without a separator are drawn in Figs. 2a, b, respectively, where the resistivity of the separator is assumed to be 100 times as large as that of the solution. The corresponding current distributions at the working- and counter-electrodes are depicted in Fig. 3. The current density increases rapidly in the vicinity of the corners of E and F owing to the edge effect. The current density decreases progressively with distance of the working-electrode from the counter-electrode.

In the absence of a separator, the current concentrates on the FG-side and the confronted part of the counter-electrode. In the presence of a separator, the current distribution becomes relatively uniform because the current density is mainly controlled by the high resistivity of the separator. In other words, the separator behaves as if it were a uniform current source. As a result, the currents at the DE and EF sides increase in comparison with those without a separator.

The current densities at the corners, E and F, should be infinite from the theoretical point of view. However, the values at E and F in Fig. 3 are finite because they are averaged around the

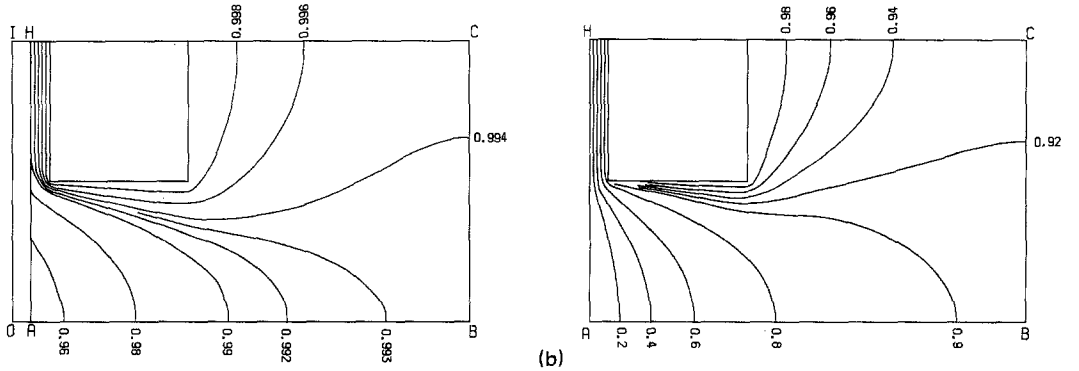

Fig. 2. Potential distributions in the cell with the following parameters: $d_1/p = 0.033$, $w/p = 0.5$, $t/p = 0.25$ and $b/p = 0.5$ when the separator is (a) present and (b) absent. The thickness and the resistivity of the separator are $d_2/p = 0.033$ and $\rho_2/\rho_1 = 100$, respectively.

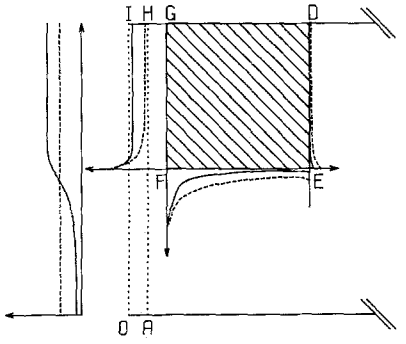

Fig. 3. Current distributions at the working- and counter-electrodes in the cells corresponding to Figs. 2a, b. The coordinates of the current densities are taken to be perpendicular to the electrode surfaces. The solid lines are for the cell without the separator ($d_2 = 0$) while the dashed lines are for the cell with the separator ($d_2/p = 0.033$ and $\rho_2/\rho_1 = 100$).

corners by the linear interpolation employed in the finite element method.

4.2. *Dependence of the unit-cell resistance on the per cent open area, o_p, and the distance, d_1*

An equivalent cell resistance, R, per unit cell is defined by

$$R = \phi^*/I \qquad (13)$$

where I is evaluated by Equation 12. In Figs. 4a–c, variations of the equivalent cell resistance with the per cent open area are shown for various values of d_1/p, $s = 2$ and $d_2/p = 0.033$ when values of ρ_2/ρ_1 are 100, 10 and 1, respectively. Since zero per cent open area corresponds to two parallel electrodes of the same size, the cell resistance is calculated on the basis of the simple uniform current distribution, as follows

$$R = (\rho_2 d_2 + \rho_1 d_1)/(p/2) \qquad (14)$$

As values of the per cent open area increase, the cell resistance is increased in concave form because the electrode parts ineffective for electrolysis (EF and DE sides) increase at the expense of the effective part (FG side).

When d_1 values are large, the profile of the current distribution can be determined by the resistance of the solution phase alone. Indeed, when values of d_1/p are larger than 0.15, the cell resistances subtracted from these of zero per cent open area are almost identical with each other regardless of the existence of the separator. We sought a

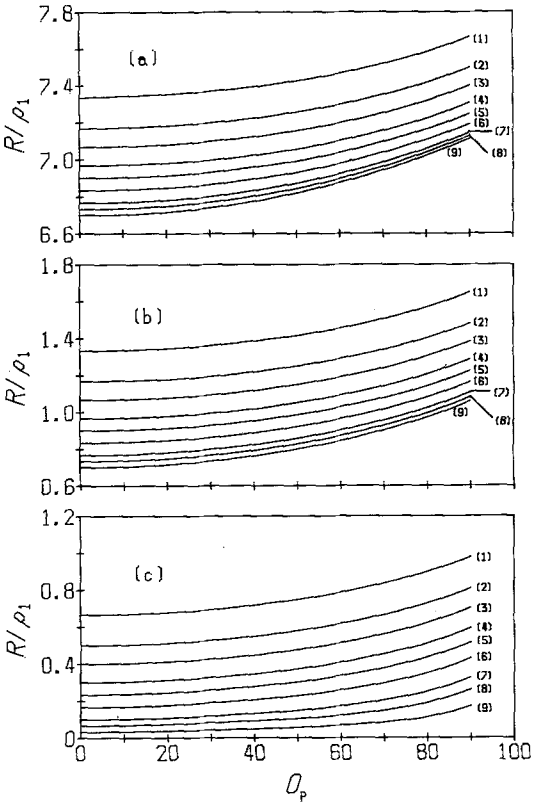

Fig. 4. Variations of cell resistance with per cent open area for $s = 2$; $d_2/p = 0.033$; $d_1/p =$ (1) 0.33, (2) 0.25, (3) 0.2, (4) 0.15, (5) 0.117, (6) 0.083, (7) 0.05, (8) 0.033, (9) 0.017; and $\rho_2/\rho_1 =$ (a) 100, (b) 10 and (c) 1.

simple expression for such curves and obtained the following approximate equation:

$$R = (\rho_2 d_2 + \rho_1 d_1)(p/2) + 0.333(o_p/100)^{2.1}\rho_1 \qquad (15)$$

This equation is valid for $o_p < 80\%$ and $d_1/p > 0.13$ within 2% error. It indicates that the cell resistance can be expressed by the sum of the interelectrode resistance and the resistance of the open part. Electrode geometry is a significant factor in cell resistance in the case of a small interelectrode resistance.

When values of d_2 are changed keeping constant the resistance of the separator, $\rho_2 d_2$, the cell resistance may be varied due to a change in the current distribution within the separator. However, it is found that the cell resistance remains almost constant providing that $\rho_2/\rho_1 > 10$ and $0.3 < (\rho_2/\rho_1)(d_2/p) < 3.5$.

The curves in Fig. 4 do not vary greatly with superficial surface area when s is larger than 1.5, as described in the next section.

4.3. *Effects of* t *and* b *on the unit-cell resistance*

The contribution of variations in the thickness of the electrode t to the equivalent unit-cell resistance R is less than 3% under the conditions that $o_p < 60\%$, $s > 1$ and $d_1/p > 0.033$ whether the cell has a separator or not. Examination of the dependence of R on b demonstrated that variations of R with b are one-third as small as those with t. Most of the real production-type cells satisfy the above conditions. Consequently t and b, especially b, have negligible effects on variations of R though they have some effects on the current distributions on the FG and EF sides.

4.4. *Partial currents at three sides of the electrode*

Of interest is the sum of the current density at each side of the working-electrode. In Fig. 5a, the partial currents at three sides in the absence of a separator are plotted vs the per cent open area for $d_1/p = 0.033$ and four values of the superficial surface area. This figure indicates that electrolysis occurs predominantly on the FG side. Therefore, concentration variations of reactants and products become large in the interelectrode region and hence concentration overvoltage at the FG side must be taken into account when one estimates the cell resistance.

In Fig. 5b, the partial currents in the presence of a separator are plotted vs the per cent open area when $d_1/p = 0.033$ and $\rho_2/\rho_1 = 100$. The variations of the partitions with per cent open area are larger than those observed in Fig. 5a. With an increase in o_p, the partitions at the FG and DE sides decrease linearly while the partition at the EF side increases. The linear dependence of the partition at the FG side on o_p results from the linear decrease in the length of FG, i.e. the decrease in the electrode area. Hence the partition at the FG side is almost independent of values of the superficial surface area. The fact that the sum of the partitions at the DE and EF sides is proportional to o_p indicates that the part of the void with length $(p - w)/2$ behaves as if it were the electrode with a slightly worse performance than the performance for the FG side.

Figs. 5a, b may be helpful for estimating amounts of electrolysis products and reactants at the three sides of the electrode.

4.5. *Average current density on three sides of the electrode*

An economically viable electrolysis process requires not only a reduction of the cell resistance but also durability of the electrode. Since in most cases, the durability of the electrode is strongly dependent on current density, uniform current density over the electrode is the most favourable condition for durability. As a measure of the

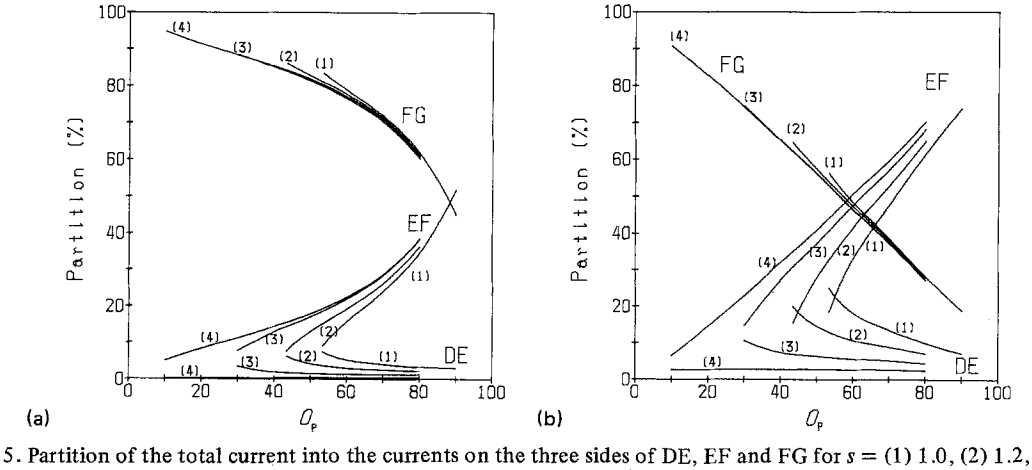

Fig. 5. Partition of the total current into the currents on the three sides of DE, EF and FG for s = (1) 1.0, (2) 1.2, (3) 1.5 and (4) 2.0 in cells (a) without and (b) with the separator of $\rho_2/\rho_1 = 100$.

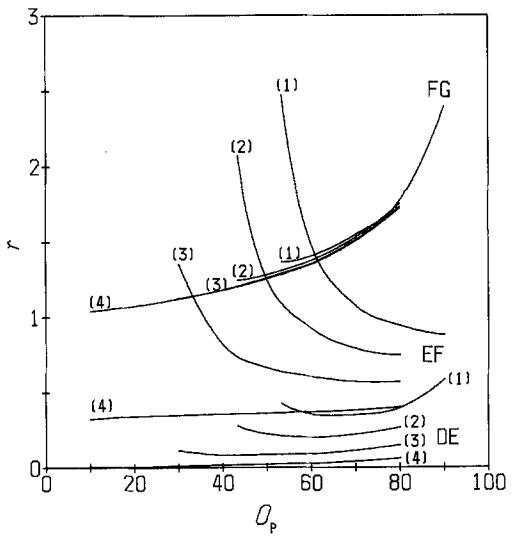

Fig. 6. Ratio of the average current density on the three sides of DE, EF and FG to that of the counter-electrode for s = (1) 1.0, (2) 1.2, (3) 1.5 and (4) 2.0 for ρ_2/ρ_1 = 10.

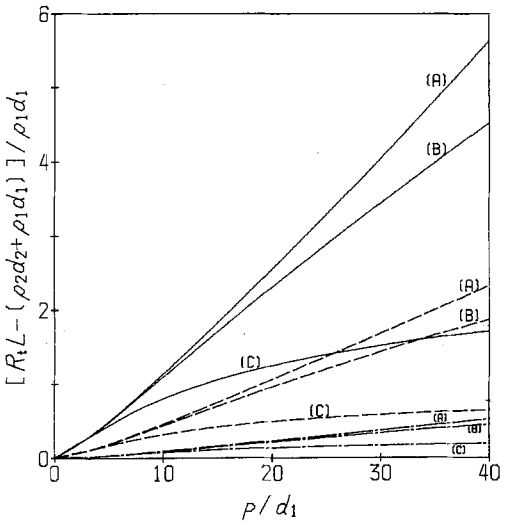

Fig. 7. Plots of the total cell resistance against the pitch for o_p = 25% (–·–), 50% (– – –), 75% (——), ρ_2/ρ_1 = (A) 100, (B) 10 and (C) 1 and t/d_1 = 15.

durability, we calculated the average current density on the DE, EF and FG sides.

In Fig. 6, the ratio of the average current density on each side to the average current density at the counter-electrode, r, is shown for some values of the superficial surface area when $d_1/p = 0.033$ and $\rho_2/\rho_1 = 10$. The average current density at the FG side varies slightly with the superficial surface area whereas variations of the current density at the EF side with o_p depend remarkably on the superficial surface area. The large values of r at the EF side result from the edge effect because such combinations of o_p and s describe very thin electrodes. If r is assumed to be a measure of a long electrode life, an electrode with a small value of r is desirable for durability. For example, electrodes with regions of $s > 1.6$ at $o_p = 30\%$, $s > 1.3$ at $o_p = 50\%$ and $s > 1.0$ at $o_p = 70\%$ may have a good durability. The curves for the other values of d_1/p and ρ_2/ρ_1 show variations similar to those in Fig. 6.

4.6. *Effect of pitch on total cell resistance*

A cell with a definite length L can be constructed with a combination of either a large number of small unit cells or a small number of large unit cells. One problem is: which combination is preferable for electrolysis? The question can be reduced to the effects of the pitch on the unit-cell resistance. The effects are revealed by varying values of p/L and w/L simultaneously keeping values of o_p, p_1, p_2, d_1, d_2, t and b constant, i.e. by expanding the cell only in the direction of the y-axis. In Fig. 7, the total cell resistance, R_t, subtracted from the cell resistance caused in the interelectrode region are plotted against p/d_1 for several values of the per cent open area. When p/d_1 values are small, the total cell resistance is expressed by

$$R_t = R(p/2L) = (\rho_2 d_2 + \rho_1 d_1)/L + 0.167(o_p/100)^{2.1}\rho_1 p/L \qquad (16)$$

The curves in Fig. 7 and this equation indicate that as the p value approaches zero, the cell resistance tends to values of the resistance between two parallel electrodes, which is the most preferred geometry for electrolysis. Therefore, making the unit cell small leads to a reduction of the cell resistance. However, a real cell composed of extremely small unit cells might make the cell resistance high because it necessarily makes the absolute size of voids small and thus the specific resistance in the interelectrode gap becomes high due to an accumulation of gas. Therefore there exists an optimum size of the pitch.

Acknowledgement

The authors wish to express their appreciation for fruitful suggestions by Mr Hiroshi Asano, Manager of Research and Development Center, Permelec Electrode Ltd.

References

[1] C. Kasper, *Trans. Electrochem. Soc.* **78** (1940) 131.
[2] *Idem, ibid.* **78** (1940) 147.
[3] *Idem, ibid.* **82** (1942) 153.
[4] S. Ishizaka and H. Matsuda, *Denkikagaku* **19** (1951) 89.
[5] H. Matsuda and S. Ishizaka, *ibid.* **20** (1952) 38.
[6] *Idem, ibid.* **20** (1952) 84.
[7] S. Ishizaka, H. Matsuda and Y. Wada, *ibid.* **22** (1954) 420.
[8] C. Wagner, *J. Electrochem. Soc.* **98** (1951) 116.
[9] *Idem, ibid.* **99** (1952) 1.
[10] F. Hine, *ibid.* **103** (1956) 186.
[11] L. E. Vaaler, *J. Appl. Electrochem.* **9** (1978) 21.
[12] C. W. Tobias, *J. Electrochem. Soc.* **106** (1959) 833.
[13] R. E. de la Rue and C. W. Tobias, *ibid.* **106** (1959) 827.
[14] P. J. Sides and C. W. Tobias, *ibid.* **127** (1980) 288.
[15] *Idem, ibid.* **129** (1982) 2715.
[16] F. Hine, M. Yasuda, R. Nakamura and T. Noda, *ibid.* **122** (1975) 1185.
[17] F. Hine, M. Yasuda, M. Watanabe and M. Kurata, *Soda to Enso (Soda and Chlorine)* **7** (1981) 281.
[18] H. Hine and K. Murakami, *J. Electrochem. Soc.* **127** (1980) 292.
[19] *Idem, ibid.* **128** (1981) 64.
[20] Z. Nagy, *J. Appl. Electrochem.* **6** (1976) 171.
[21] A. T. Kuhn, J. B. Yusof and P. Hogan, *ibid.* **9** (1979) 765.
[22] G. Kreysa and H-J. Külps, *J. Electrochem. Soc.* **128** (1981) 979.
[23] J. Jorne and J. F. Louvar, *ibid.* **127** (1980) 298.
[24] L. J. J. Janssen, J. J. M. Geraets, E. Barendrecht and S. D. J. van Stralen, *Electrochim. Acta* **27** (1982) 1207.
[25] H. Vogt, *J. Appl. Electrochem.* **13** (1983) 87.
[26] O. Lanzi and R. F. Savinell, *J. Electrochem. Soc.* **130** (1983) 799.
[27] R. Alkire, T. Bergh and R. L. Sani, *ibid.* **125** (1978) 1981.
[28] R. Sautebin, H. Froidevaux and D. Landolt, *ibid.* **127** (1980) 1096.
[29] T. Gueshi, K. Tokuda and H. Matsuda, *Denki-kagaku* **51** (1983) 107.
[30] O. C. Zienkiewicz, 'The Finite Element Method', McGraw-Hill, London (1977).
[31] E. Jasse and E. Ziganke, *Arch. Electrochem.* **22** (1929) 177.